RSC Advances

ROYAL SOCIETY
OF CHEMISTRY

www.rsc.org/advances

1　**PbCl$_2$-assisted film formation for high-efficiency heterojunction perovskite solar cells**

2　Si Chen[a], Xiao Yu[a], Xin Cai[a], Ming Peng[a], Kai Yan[a], Bin Dong[a], Hsienwei Hu[a], Buxin Chen[a], Xue

3　Gao[a] and Dechun Zou[a,b,]*

4　 [*] Prof. Dechun Zou (E-mail: dczou@pku.edu.cn)

5　[a]Beijing National Laboratory for Molecular Sciences, Key Laboratory of Polymer Chemistry and

6　Physics of Ministry of Education, Center for Soft Matter Science and Engineering, College of

7　Chemistry and Molecular Engineering, Peking University, Beijing 100871, China.

8　Tel/Fax: +86-10-6275-9799.

9　[b]Beijing Engineering Research Center for Active Matrix Display, Peking University,

10　Beijing 100871, China.

11

12　**Abstract**

13　　In this work, PbCl$_2$ is used as an additive to assist organolead trihalide perovskite film

14　formation in two-step sequential deposition. PbCl$_2$ inhibits PbI$_2$ crystallization and contributes to

15　the full conversion of PbI$_2$ and enhanced perovskite film morphology control. Cl$^-$ incorporation

16　into perovskite improves charge transport within the film, as confirmed by the resulting prolonged

17　photoluminescence lifetime observed. A reaction temperature of approximately 50 °C between the

18　PbI$_2$/PbCl$_2$ film and CH$_3$NH$_3$I isopropanol solution is essential for synthesizing high-performance

19　perovskite solar cells. Addition of PbCl$_2$ results in a perovskite solar cell energy efficiency of 14%

20　and achieves in average efficiency enhancement of approximately 30% compared with that

21　obtained from the control group.

22　**Keywords**

23　　PbCl$_2$ additive, two-step sequential deposition, heterojunction, perovskite solar cells

24　**Introduction**

25　　Organic-inorganic hybrid perovskite solar cells are an emerging photovoltaic technology. These

26　devices have gained much attention since the first solid perovskite solar cell were first reported in

1   2012 to have power conversion efficiencies (*PCEs*) of 10%[1, 2]. Perovskite solar cells have

2   exhibited rapid development within the last three years, and a remarkable high efficiency of over

3   19% has been achieved[3]. The early perovskite solar cells were mostly solid mesoporous solar cells

4   in which perovskite materials, such as $CH_3NH_3PbI_3$ and $CH_3NH_3PbI_{3-x}Cl_x$, were often deposited

5   on mesoporous scaffolds, such as TiO_2 and Al_2O_3. Subsequent studies showed that organolead

6   trihalide perovskite can function as exceptional panchromatical-light absorbing materials[4-7],

7   efficiently facilitate charge separation, and react as both electron and hole transporters. These

8   characteristics are due to the ambipolar semiconducting nature of the perovskite, which enables

9   fabrication of efficient planar heterojunction devices. Compared with mesoporous structured

10   devices, planar heterojunction devices simplify the fabrication processes and are more attractive

11   for developing flexible and tandem solar cells[7]. Several methods have been developed to achieve

12   high-performance planar heterojunction perovskite solar cells. The earliest report of such a method

13   adopted a dual-source evaporation technique to prepare a high-quality perovskite layer by

14   co-evaporation of $PbCl_2$ and CH_3NH_3I and obtained a *PCE* of as high as 15.4%[8]. However, the

15   requirements of high vacuum conditions and sophisticated equipment are unfavorable for the

16   large-scale fabrication of these devices.

17

18   Two-step sequential deposition of perovskite has also been used to fabricate planar

19   heterojunction devices. This technique features improved control of the perovskite film

20   morphology. Two-step sequential deposition of $(RNH_3)_2(CH_3NH_3)_{n-1}M_nI_{3n+1}$ (R=butyl, phenethyl;

21   M=Pb, Sn) perovskite film was first reported by Mitzi *et al.*[9] and successfully developed by

22   Grätzel et al.[10] for $CH_3NH_3PbI_3$ synthesis. This deposition technique was first applied to

23   mesoporous structured devices with a scaffold layer in the early reach stages, such as TiO_2 or

24   Al_2O_3. During two-step deposition, a high-concentration PbI_2 solution is first spin-coated onto the

25   substrate and then reacted with CH_3NH_3I. Two-step sequential deposition can be categorized into

26   two according to the treatment in the second step. Thus, deposition can either be a vapor-assisted

27   solution process (VASP) or a solution-based process that includes dipping[10] and interdiffusion[11]

28   methods.

1   VASP was first developed by Yang *et al.*[12]. A PbI_2 thin film prepared by spin-coating was

2   reacted with CH_3NH_3I vapor at 150 °C to convert the thin film into perovskite, leading to a *PCE*

3   of 12.1%. The resulting *PCE* was further enhanced to 16.8%[13] by lowering the reaction

4   temperature and CH_3NH_3I vapor pressure. In this work the beneficial effect of using mixed

5     $PbI_2/PbCl_2$ precursor in two step process has also been demonstrated[13]. Except that the use of

6   mixed $PbI_2/PbBr_2$ precursor solution for a sequential deposition process has also been

7   demonstrated[14]. Compared with VASP, the second type of deposition solution process is easier to

8   operate and considerably more accessible to diverse perovskite devices. However, the good

9   crystallinity of PbI_2 produces undesirable effects. The PbI_2 crystal size is confined by the space

10   between nanoparticles in the mesoporous structure but preferably forms large crystals in the planar

11   heterojunction structure. Considering that the second reaction with CH_3NH_3I is a heterogeneous

12   reaction, large PbI_2 crystals will feature reduced accessibility to small organic molecules, thereby

13   resulting in incomplete PbI_2 conversion. This phenomenon can severely impact device efficiency

14   and reproducibility. Additionally, variations in PbI_2 crystal size lead to changes in the perovskite

15   crystal size, which probably contributes to uncontrollable film morphologies. When

16   *N,N*-dimethylformamide (DMF) solvent is replaced with dimethyl sulfoxide (DMSO), the

17   molecules of which have stronger coordination with Pb^{2+} than DMF, PbI_2 crystallization can be

18   effectively inhibited, leading to full conversion of PbI_2[15]. Consequently, high-efficiency

19     $CH_3NH_3PbI_3$ perovskite solar cells with enhanced reproducibility are obtained.

20   To the best of our knowledge, the use of Cl^- as a dopant agent can result in formation of

21     $CH_3NH_3PbI_{3-x}Cl_x$ and greatly improve the transport properties of perovskite, especially its

22   hole/electron diffusion length. Cl^- can also induce lattice distortion during perovskite

23   crystallization, which slows down the crystal growth rate[16]. This phenomenon is mainly inferred

24   from the longer annealing time and higher annealing temperature required for full conversion into

25   perovskite compared with pure PbI_2-based materials. In this work, we presented $PbCl_2$ as an

26   additive and adopted interdiffusion of spun stacking layers of PbI_2/PbI_2 and CH_3NH_3I to fabricate

27   perovskite solar cells[11]. The $PbCl_2$ additive effectively inhibited crystallization of PbI_2 to complete

28   its conversion of PbI_2 and controlled the resulting $CH_3NH_3PbI_{3-x}Cl_x$ film morphology.

1   Introduction of PbCl$_2$ dramatically prolonged the fluorescence lifetime of perovskite, indicating

2   improved charge transport properties within the perovskite layer. The system with PbCl$_2$ additive

3   was more sensitive to the spin-coating temperature of the CH$_3$NH$_3$I/isopropanol solution than that

4   without the additive. Higher temperatures benefited formation of larger perovskite crystal sizes,

5   which remarkably enhanced fill factor (*FF*) and J_{sc}. Adjusting the amount of PbCl$_2$ and further

6   optimizing the spin-coating temperature resulted in enhancements in the average *PCE* of the

7   corresponding perovskite solar cells by over 30% compared with that of pure PbI$_2$-based devices.

8   **Results and discussion**

9   The preparation of perovskite film on glass substrate is illustrated in Figure 1a. Various molar

10   ratios of PbI$_2$ and PbCl$_2$ were dissolved in DMF, spin-coated onto cleaned FTO at 70 °C, and then

11   annealed at 100 °C for 60 min to exclude the DMF molecules. Then, 40 mg/mL CH$_3$NH$_3$I in

12   isopropanol solution was hot-casted onto the as-prepared PbI$_2$/PbCl$_2$ thin film, followed by solvent

13   annealing treatment for 60 min at 100 °C. Eventually, spiro-MeOTAD was spin-coated onto the

14   top of the substrate as a hole-transporting material. The Au counter electrode was formed *via*

15   magnetron sputtering. The device structure adopted in the current study was

16   FTO/cTiO$_2$/CH$_3$NH$_3$PbI$_{3-x}$Cl$_x$/spiro-MeOTAD/Au. A cross-sectional view of the device is shown

17   in Figure 1b.
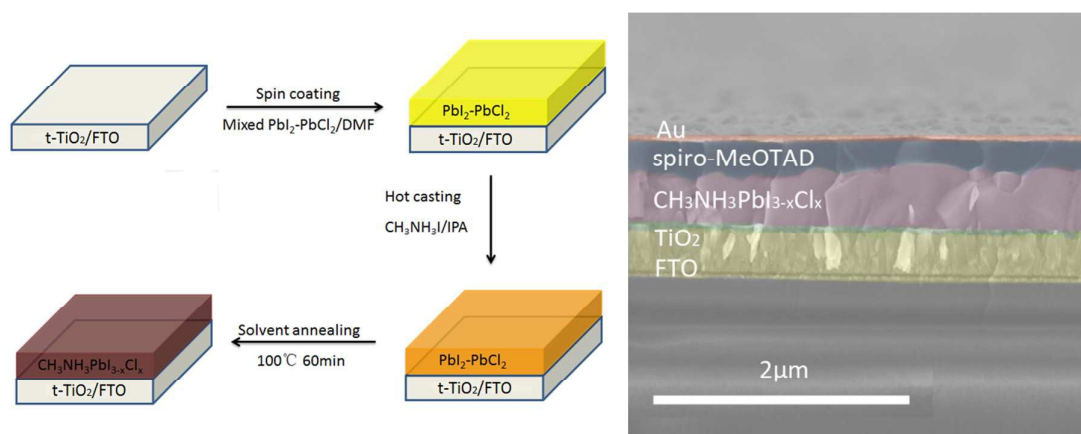
18

19   **Figure 1** a. Schematic of the preparation process of perovskite film (t-TiO$_2$ referred to the TiO$_2$

20   compact layer). b. Scanning electron micrograph of the cross-sectional view of the perovskite

1   solar cell

2

3   We found that the temperature of the FTO substrate and PbI_2-$PbCl_2$/DMF solution influenced

4   the final morphology of the perovskite film during spin-coating of the PbI_2-$PbCl_2$/DMF solution.

5   Figure S1 shows a scanning electron micrograph of the film spin-coated from PbI_2-$PbCl_2$/DMF

6   solution with 33% molar ratio of $PbCl_2$ at room temperature and then annealed at 100 °C for

7   60 min. The morphology of this film remarkably differed from that of the film spin-coated at

8   higher temperatures (70 °C; Figure S1b). Lower temperatures induced the formation of smaller

9   crystal sizes and higher porosity, which are not beneficial to the morphological control of the

10   perovskite film. Warmer substrates and precursors may contribute to PbI_2 crystallization,

11   consistent with other reports that adopted a temperature of 70 °C to spin-coat PbI_2/DMF solution

12   during the two-step sequential deposition process[8, 17]. The morphologies of PbI_2/$PbCl_2$ films with

13   varied molar ratios of $PbCl_2$, which are shown in Figures S2a–S2c, are clearly distinguishable

14   from those of pure PbI_2 film, which is composed of large flaky crystals, as illustrated in Figure

15   S2d. Addition of $PbCl_2$ apparently changed the film morphology by diminishing the PbI_2/$PbCl_2$

16   crystal size and smoothing the film surface to decrease roughness. When the molar ratio was

17   further increased to 50%, film coverage decreased and porosity evidently increased.

18   Well-regulated PbI_2/$PbCl_2$ films generally favor the formation of high-quality perovskite film[8, 17].

19   Therefore, addition of an appropriate molar ratio of $PbCl_2$ is necessary for morphological control

20   of subsequent perovskite film.

21   When the amount of $PbCl_2$ added was increased from 0% to 50%, the color of the prepared

22   PbI_2/$PbCl_2$ film on prepared substrate changed from yellow to white (Figure S3). This change was

23   further demonstrated by the UV-vis absorption spectra of PbI_2/$PbCl_2$ films on substrate with

24   different molar ratios of $PbCl_2$. The pure PbI_2-based film revealed an absorption peak centered at

25   500 nm (Figure 2a), which is attributed to the band-gap excitation of crystallized PbI_2. The

26   absorption intensity of the characteristic peak weakened with increasing amount of added $PbCl_2$.

27   The absorption peak at 500 nm disappeared at 50% $PbCl_2$ molar ratio. This phenomenon basically

28   proves the amorphous nature of PbI_2. XRD patterns of the PbI_2/$PbCl_2$ films (Figure 2b) also

1   verified the inhibition effect of $PbCl_2$ on PbI_2 crystallization. PbI_2 films exhibited a strong

2   diffraction peak at $2\theta=12.6°$, which corresponds to the (001) crystal plane of crystallized PbI_2. The

3   intensity of this characteristic peak significantly decreased when $PbCl_2$ was introduced to the

4   system and completely disappeared in the XRD pattern of $PbI_2/PbCl_2$ film when the $PbCl_2$ molar

5   ratio was increased to 50%. The absence of this characteristic diffraction peak indicates that the

6   film is in an amorphous state. The inhibitory effect of $PbCl_2$ may be ascribed to the formation of a

7   new phase (PbClI) which can be identified by XRD pattern of the film. By Comparing the XRD of

8     $FTO/cTiO_2/PbI_2:PbCl_2$ and $FTO/cTiO_2$ (figure 2c), we can found that peaks $2\theta=26.4°$, $37.8°$, $51.4°$

9   belongs to the substrate of $FTO/cTiO_2$. And according to previous report[13, 18] relatively weak peaks

10   at $21.34°$, $28.9°$, $30.7°$, and $34.1°$, corresponding to the (120), (121), (211), and (310) crystal

11   planes of PbClI(Figure 2c). The new double peaks at $2\theta=23.6°$ and $24.0°$ also appeared at the

12   XRD pattern of $PbI_2/PbCl_2$ based on other $PbCl_2$ of other molar ratios which we believe might be

13   assign to the intermediate phase of $PbCl_2/PbI_2$ formed during preparation process. Taken together,

14   the UV-vis absorption spectra and XRD patterns confirm the inhibitory effects of $PbCl_2$ on PbI_2

15   crystallization; such inhibition may accelerate the reaction between $PbI_2/PbCl_2$ film and organic

16   CH_3NH_3I molecules[16].

17   We compared the evolutional processes of the XRD patterns of perovskite films based on

18     $PbI_2/PbCl_2$ (33% molar ratio of $PbCl_2$) (Figure 2d) and pure PbI_2-based (Figure S4) films at

19   different annealing times. The perovskite peak intensity was fairly weak immediately after

20   spin-coating, especially in the pure PbI_2-based sample. This finding suggests that both pure PbI_2

21   and $PbI_2/PbCl_2$ films without annealing cannot completely react; such a phenomenon is supported

22   by the scanning electron micrograph showing unreacted $PbI_2/PbCl_2$ phase in Figure S5. After

23   annealing at 100 °C for 15 min, the pure PbI_2 sample still showed diffraction peaks at $2\theta = 12.6°$,

24   indicating residual unreacted PbI_2. The peak intensity of PbI_2 continued to decrease until an

25   annealing time of 30 min. The small PbI_2 peak was maintained even after 60 min, thereby

26   implying incomplete conversion of PbI_2. In the $PbI_2/PbCl_2$ samples, the small PbI_2 peak

27   disappeared immediately after spin-coating, and the intensity of the perovskite film remained

28   nearly unchanged after 15 min; no characteristic peak of PbI_2 was observed at $2\theta = 12.6°$. The

1   peak of the PbClI phase completely disappeared, likely because of reaction between PbClI phase

2   and MAI that convert into perovskite. These findings indicate that addition of $PbCl_2$ facilitates the

3   reaction between PbI_2 and CH_3NH_3I.
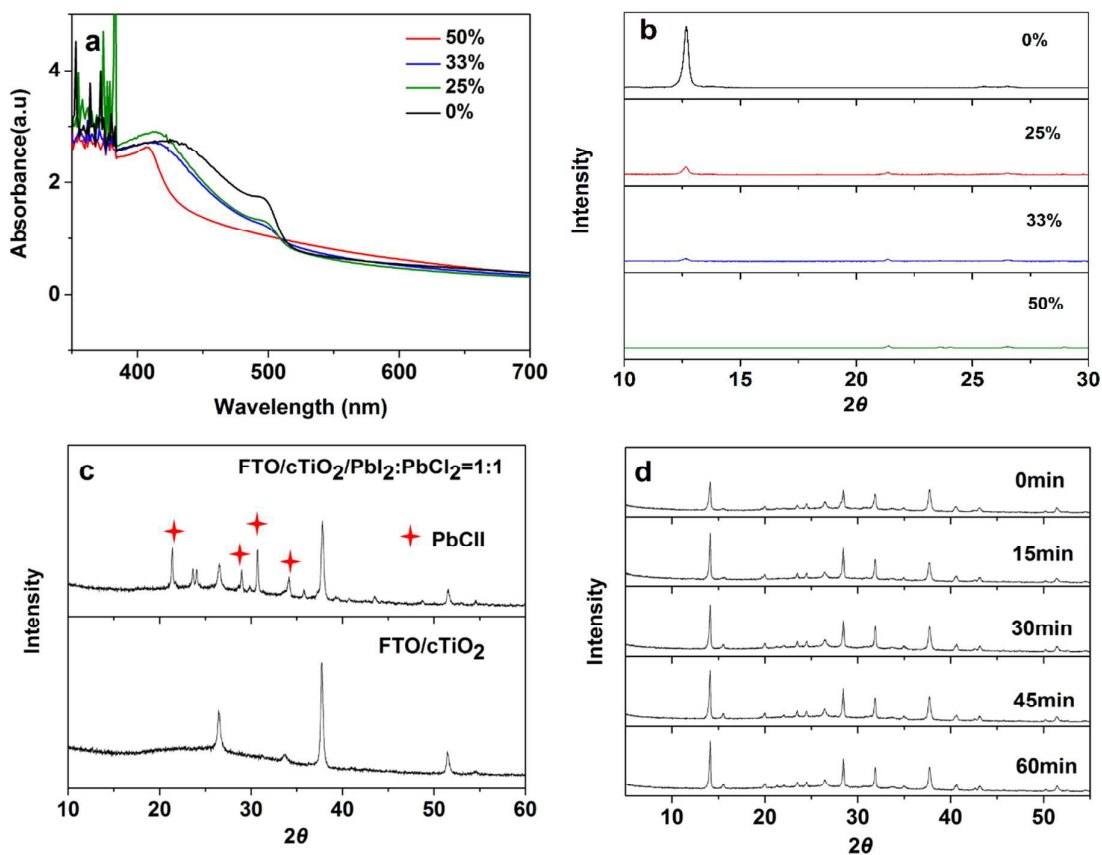
4

5   **Figure 2** UV-vis absorption spectra (a) and XRD patterns (b) of $PbI_2/PbCl_2$ films based on

6   different $PbCl_2$ molar ratios (adopted structure, $FTO/cTiO_2/PbI_2$-$PbCl_2$). (c) XRD patterns of 50%

7    $PbCl_2$ molar ratio $PbI_2/PbCl_2$ film and the control sample. (d) XRD patterns of perovskite films

8   obtained from 33% $PbCl_2$ molar ratio $PbI_2/PbCl_2$ films obtained at different annealing times

1
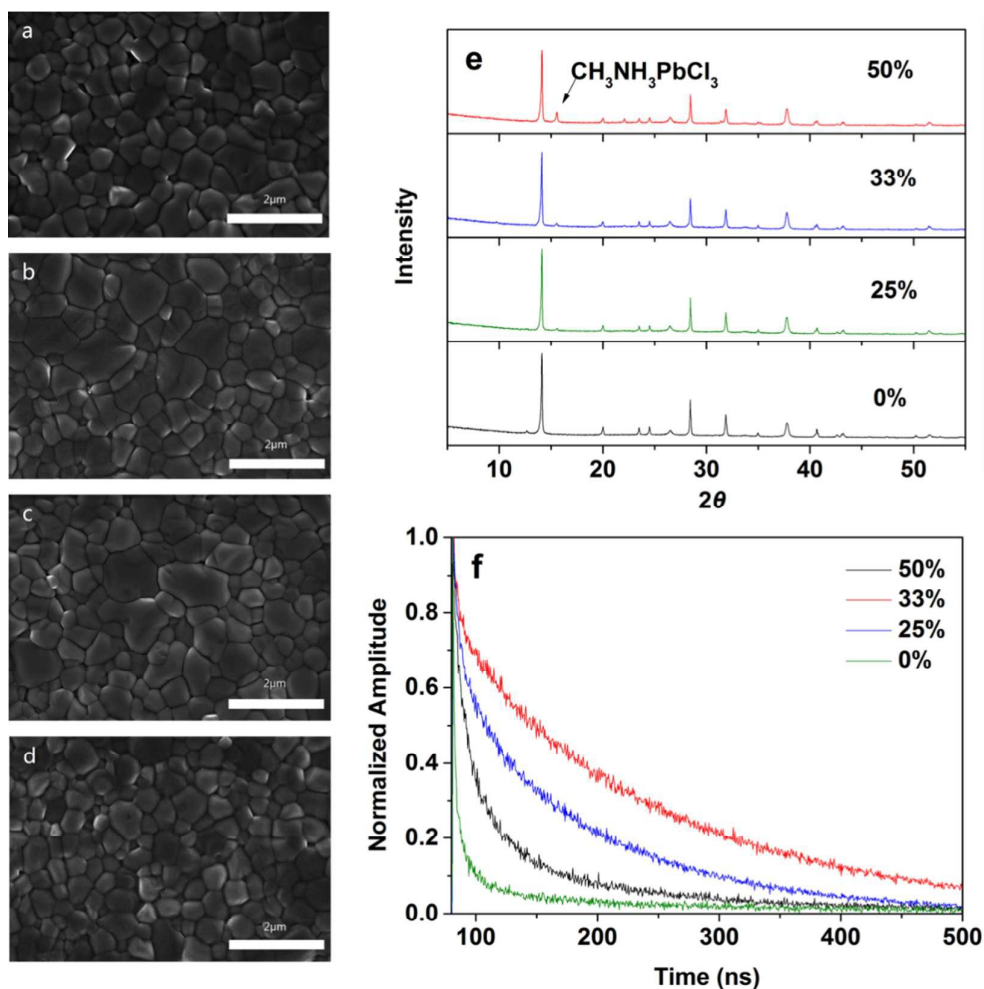
Figure 3 Scanning electron micrographs of perovskite films based on $PbI_2/PbCl_2$ films with $PbCl_2$
molar ratios of (a) 50%, (b) 33%, (c) 25%, and (d) 0%. (e) XRD patterns of perovskite films based
on $PbI_2/PbCl_2$ films with different $PbCl_2$ molar ratios. (f) Time-resolved photoluminescence decay
plot of perovskite films based on $PbI_2/PbCl_2$ films with different $PbCl_2$ molar ratios. The
excitation wavelength was 440 nm and the probe wavelength was 780 nm.

$PbCl_2$ inhibited PbI_2 crystallization and assisted in the completion of the PbI_2 reaction. Hence,
we supposed that addition of $PbCl_2$ may play an important role in perovskite formation and device
performance. Thus, we examined the property of perovskite films based on $PbI_2/PbCl_2$ films with
varying amounts of $PbCl_2$. We found that all of the $PbI_2/PbCl_2$ films formed perovskite after

1 solvent annealing treatment. Figures 3a–3d show the scanning electron micrographs of perovskite

2 based on $PbI_2/PbCl_2$ films of different molar ratios. The resulting perovskite demonstrated larger

3 crystal sizes and enhanced smoothness compared with the thermally annealed sample as a result of

4 the solvent annealing process (Figure S6). The morphology of the perovskite films showed no

5 distinct difference, probably because of solvent annealing. When the added amount of $PbCl_2$ was

6 excessively high or no $PbCl_2$ was added, the grain size and smoothness decreased to a certain

7 extent, likely because of morphological differences in the $PbI_2/PbCl_2$ films discussed above[1, 2, 13].

8 The XRD patterns of the perovskite films (Figure 4e) formed from $PbI_2/PbCl_2$ films of different

9 $PbCl_2$ molar ratios showed peaks at 2θ = 14.08°, 28.5°, 31.8°, and 43.2°, respectively

10 corresponding to the (110), (220), (310), and (330) crystal planes of perovskite. No apparent

11 differences were found between the peak positions of $CH_3NH_3PbI_{3-x}Cl_x$ and $CH_3NH_3PbI_3$, in

12 agreement with other reportes[13, 19].

13 EDS (Energy Dispersive X-ray Spectrometer) results show that $CH_3NH_3PbI_{3-x}Cl_x$ also exhibits

14 no detection signal of Cl because of content of Cl below the LOD (limit of detection which is

15 about 1% atomic percentage) of EDS (Figure S7)[17, 20, 21]. According the previous report that the

16 measurement result delivered by XPS (X-ray photoelectron spectroscopy) of Cl atomic percentage

17 in $CH_3NH_3PbI_{3-x}Cl_x$-based perovskite is about 0.7%[17, 21]. Compared with the XRD patterns of

18 perovskite films based on $PbI_2/PbCl_2$ films with different molar ratios (Figure 4e), the pure

19 PbI_2-based perovskite film showed the residual characteristic peak of PbI_2 at 2θ = 12.6°,

20 indicating incomplete conversion of PbI_2. When $PbCl_2$ was introduced to the system, new

21 diffraction peak at 2θ = 15.5° appeared. According to the previous work[19, 22, 23], this diffraction

22 peak corresponds to the $CH_3NH_3PbCl_3$ phase with clear identification, and this which also appears

23 in other $CH_3NH_3PbI_{3-x}Cl_x$-based perovskite XRD patterns[5, 13, 17, 23]. When the amount of added

24 $PbCl_2$ was increased, the characteristic peak intensity of $CH_3NH_3PbCl_3$ was enhanced. At 50%

25 $PbCl_2$, an obvious peak at 2θ = 15.5° appeared in the XRD pattern (Figure 4e). The scanning

26 electron micrographs and XRD patterns prove that $PbI_2/PbCl_2$ films with different $PbCl_2$ molar

27 ratios could form perovskite films. Excessively high or too low $PbCl_2$ molar ratios resulted in

28 decreased grain sizes and smoothness. Addition of $PbCl_2$ also led to the formation of the

1    $CH_3NH_3PbCl_3$ phase.

2   We investigated the photovoltaic parameters of solar cells based on different $PbCl_2$ molar ratios,

3   and the results are summarized in Table 1 and Figure 4; statistical data derived from 40 devices

4   are listed under each condition. Addition of $PbCl_2$ showed no apparent influence on the

5   open-circuit voltage, which was approximately 1 V. When the amount of $PbCl_2$ added was at a

6   certain range ($PbCl_2$ molar ratio from 0% to 33%), J_{sc} was not evidently affected. J_{sc} declined

7   distinctly only when the molar ratio of $PbCl_2$ reached 50%. This phenomenon may have been

8   caused by incomplete conversion of $PbCl_2$. The reaction between $PbCl_2$ and CH_3NH_3I usually

9   requires longer reaction time and higher reaction temperatures compared with that of PbI_2[2, 24].

10   However, the reaction time and temperature were limited during the spin-coating process. The

11   amount of CH_3NH_3I left over on top of the $PbI_2/PbCl_2$ film after spin-coating was also limited.

12   These characteristics led to incomplete conversion of $PbCl_2$. The observed phenomena could also

13   be supported by the fact that the optimized reaction temperature for $PbI_2/PbCl_2$-based devices is

14   higher than that of pure PbI_2-based ones. Addition of $PbCl_2$ evidently improved *FF* and

15   contributed to the enhancement of *PCE*. The cells presented the highest average *PCE* at a $PbCl_2$

16   molar ratio of 33%. The devices demonstrated the following characteristics: average V_{oc},

17   0.98±0.02 V; J_{sc}, 20.70±1.00 mA/cm^2; *FF,* 0.59±0.03; and *PCE,* 12.1%±0.98%. The average *PCE*

18   of the devices obtained was enhanced by 30%, from 9.3% to 12.1%, compared with that of the

19   control group.

20

21   **Table 1 Device performance of perovskite solar cells**

$PbCl_2$ molar ratio (%)	V_{oc} (V)	J_{sc} (mA/cm^2)	*FF*	*PCE* (%)
0	0.96±0.03	20.1±1.33	0.48±0.03	9.3±0.78
25	1.01±0.02	20.3±0.84	0.57±0.03	11.7±0.90
30	0.98±0.02	20.7±1.00	0.59±0.03	12.1±0.98

| 50 | 1.00±0.03 | 18.1±1.21 | 0.53±0.03 | 9.7±0.92 |

1   Under each condition, the listed result is the standard deviation calculated from 40 devices.
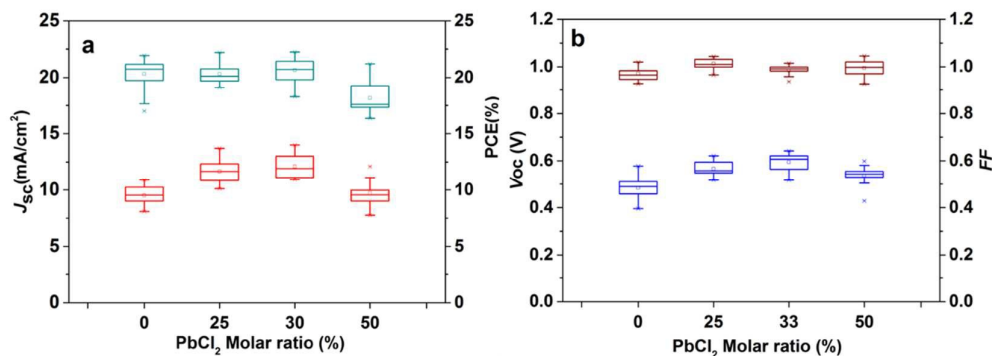
2

3   **Figure 4** Photovoltaic parameters of solar cells with different PbCl$_2$ molar ratios. Dark cyan, red,

4   brown, and blue boxes represent the photovoltaic J_{sc}, PCE, V_{oc}, and FF, respectively. Each box

5   presents the parameter distribution of 40 devices under similar working conditions. The parameter

6   values are presented as box plots for distributions of the different PbCl$_2$ molar ratios. Box edges

7   represent the 25/75 percentile. The small square symbol (□) inside the boxes represents the mean,

8   whereas the line across the boxes represents the median. The furcation symbols (×) represent the

9   maximum and minimum values.

10

11   We performed time-resolved photoluminescence (PL) measurements on the different perovskite

12   films to explore the mechanism by which PbCl$_2$ affects device performance. Time-resolved PL

13   measurements provide important information on the lifetime of the excited species in the

14   photoactive layer, which can be used to deduce the diffusion length of the charge carriers. All of

15   the test samples adopted the structure of glass/CH$_3$NH$_3$PbI$_3$ or glass/CH$_3$NH$_3$PbI$_{3-x}$Cl$_x$. The decay

16   plots obtained are shown in Figure 3f. All the testing results fit the biexponential decay dynamics,

17   and the fitted parameters are presented in Table S2. Biexponential decay maybe attributed to

18   variations in the perovskite grain size[17]. Slower decay time represent longer diffusion lengths,

19   indicating higher charge collection efficiencies. Addition of PbCl$_2$ effectively prolonged the PL

20   lifetime τ_{slow}. At a PbCl$_2$ molar ratio of 33%, the lifetime τ_{slow} reached 172.63 ns, which is far

1 longer than the 75.17 ns of τ_{slow} of the pure PbI_2-based sample. A $PbCl_2$ molar ratio higher than 33%

2 decreased the lifetime. This variation in the PL lifetime basically agrees with the variation in

3 device performance. Lifetime extension can be explained by Cl^- doping, which has been reported

4 to remarkably improve transport propert[16, 25]. Thus, addition of $PbCl_2$ can enhance device

5 performance by improving perovskite film transport properties

6 The spin-coating temperature of the CH_3NH_3I/isopropanol solution plays an important role in

7 device efficiency during device fabrication, especially when PbI_2/$PbCl_2$-based devices are

8 produced. This sensitivity to temperature may be derived from the fact that $PbCl_2$ requires higher

9 reaction temperature and longer reaction time to convert into perovskite[2, 24]. Excess Cl^- may

10 sublime in the form of CH_3NH_3Cl and leave only trace amounts of chloride in the perovskite. The

11 sublimation process would therefore influence the phase transformation process, wherein lattice

12 distortion caused by Cl^- doping and exclusion of organic molecules could improve perovskite

13 crystallization[5, 12, 26, 27]. Figure 5e shows the XRD patterns of $CH_3NH_3PbI_{3-x}Cl_x$ prepared at

14 different temperatures. When the spin-coating temperature was enhanced from 30 °C to 60 °C, the

15 peak intensity of the formed perovskite was reinforced and the half-peak width of the

16 characteristic peak at $2\theta = 14.08°$ became smaller, indicating improved perovskite crystallinity.

17 The characteristics of the perovskite films prepared at different temperatures shown in Figures 5a–

18 5d indicate that larger crystalline grains are preferred at higher temperatures, further supporting

19 the enhancement of perovskite crystallization. Compared with the XRD patterns of perovskite

20 films at spin-coating temperatures of 30 °C (Figure S8) and 50 °C (Figure 2d), the intensity of the

21 characteristic perovskite peak at $2\theta = 14.08°$ obtained immediately after 50 °C hot casting without

22 annealing was much stronger than that observed at 30 °C. This phenomenon suggests that larger

23 amounts of PbI_2/$PbCl_2$ convert into the perovskite phase before annealing treatment. Higher

24 conversion ratios of PbI_2/$PbCl_2$ may benefit the formation of larger perovskite grain sizes. When

25 the hot spin-coating temperature of the CH_3NH_3I/isopropanol solution reached 60 °C, severe

26 damage of the perovskite film surface is observed (Figure S9). This development is mainly due to

27 the restriction of the boiling temperature (82 °C) of isopropanol. High spin-coating temperatures

28 accelerate the evaporation of isopropanol and result in rapid separation of CH_3NH_3I to form

1   visible crystals. Excessive CH_3NH_3I residues may also affect device performance. Thus, reaction

2   temperatures of no more than 60 °C may ensures device performance.
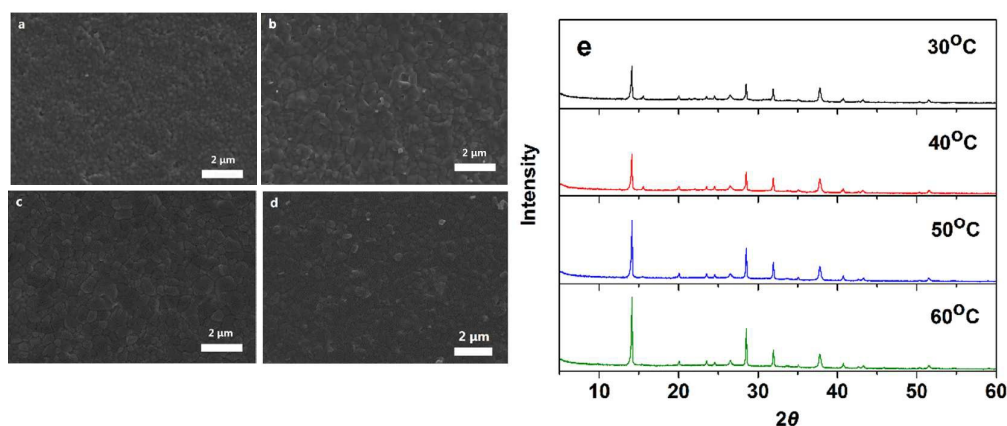
3

4   **Figure 5** Scanning electron micrographs of perovskite films prepared from 33% $PbCl_2$ molar ratio

5    $PbI_2/PbCl_2$ films based on MAI spin-coating temperatures of (a) 30 °C, (b) 40 °C, (c) 50 °C, and

6   (d) 60 °C. (e) XRD patterns of perovskite films based on 33% $PbCl_2$ molar ratio $PbI_2/PbCl_2$ films

7   with different MAI spin-coating temperatures.

8

9   The photovoltaic parameters of 40 devices for each spin-coating temperature are shown in

10   Figure S10. No apparent difference in V_{oc} was observed under the different spin-coating

11   temperatures, and values of approximately 1 V were consistently obtained. The different spinning

12   temperatures mainly affected the J_{sc} and FF values of the devices. When the temperature was

13   increased from 30 °C to 50 °C, the average J_{sc} increased from 16.68 mA/cm^2 to 20.65 mA/cm^2,

14   and the average FF increased from 0.54 to 0.59. The average J_{sc} values of devices based on

15   different spin-coating temperatures corresponded to the IPCE integral values at varied

16   spin-coating temperatures (Figure 6a). This phenomenon can be explained by the formation of

17   larger grain sizes of perovskite at higher temperatures, as confirmed by the XRD patterns and

18   scanning electron micrographs described earlier. Larger grain sizes of perovskite decrease the

19   impact of grain boundaries on charge separation and transmission. Grain boundaries, especially

20   those on the longitudinal transport pathway, induce charge recombination, which severely affected

1   the device performance[11]. Fewer grain boundaries provide effective charge transport, inhibit

2   interface charge recombination, and improve J_{sc} and FF. When the temperature was excessively

3   high, CH_3NH_3I precipitated before reacting with $PbI_2/PbCl_2$ during spin-coating, and the residual

4   CH_3NH_3I negatively affected device performance. The optimized spin-coating temperature was

5   50 °C, at which point the average PCE was enhanced by 34% compared with that at 30 °C. The

6   best device achieved a maximum PCE of 14% as well as V_{oc}, $J_{sc,}$ and FF values of 0.99 V, 21.8

7   mA/cm[2,] and 0.64, respectively (Figure 6d).
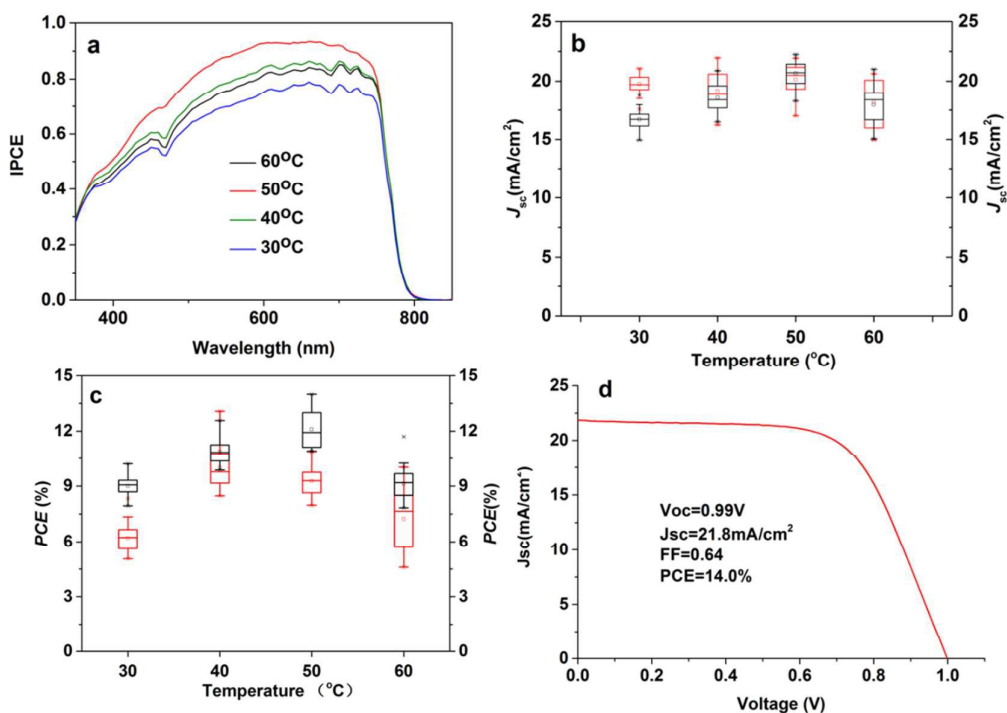
8

9   **Figure 6** (a) IPCE of perovskite solar cells based on 33% $PbCl_2$ molar ratio $PbI_2/PbCl_2$ film

10   spin-coated CH_3NH_3I solution at different temperatures. (b) J_{sc} of solar cells based on 33% $PbCl_2$

11   molar ratio (black) films and pure PbI_2 films (red) prepared from different CH_3NH_3I isopropanol

12   solution spin-coating temperatures. (c) PCE of solar cells based on 33% $PbCl_2$ molar ratio film

13   (black) and pure PbI_2 films (red) prepared from different CH_3NH_3I isopropanol solution

14   spin-coating temperatures. Each box presents the parameter distribution of 40 devices under

15   similar working conditions. The parameter values are presented as box plots of distributions for a

16   range of different $PbCl_2$ molar ratios. Box edges represent the 25/75 percentile. The small square

1   symbol (□) inside the boxes represents the mean, whereas the line across the boxes represents the

2   median. The furcation symbols (×) represent the maximum and minimum values). (d) *J-V* curve of

3   the device with highest *PCE* reverse scan. The device was spin-coated with 33% molar ratio $PbCl_2$

4   at 50 °C.

5

6   We further compared the device performances of pure PbI_2 with the $PbI_2/PbCl_2$ system obtained

7   at different CH_3NH_3I isopropanol solution spin-coating temperatures (Figure S11). Similar to

8    $PbI_2/PbCl_2$, the V_{oc} of the devices showed no apparent difference under various spin-coating

9   temperatures. However, the J_{sc} of the PbI_2-based device was not sensitive to the temperature, and

10   the average J_{sc} was approximately 20 mA/cm^2, as shown in Figure 6b. The influence of

11   temperature was mainly observed in terms of *FF*. The optimal spin-coating temperature of the

12   pure-PbI_2 device was 40 °C, which is lower than that of the $PbI_2/PbCl_2$-based device (Figure 6c),

13   and the distribution of the *PCE* of the former was wider compared with that of the latter. Under

14   optimized fabrication conditions, the average *PCE* based on $PbI_2/PbCl_2$ was enhanced by 21%

15   compared with that of the control group.

16   Photocurrent hysteresis is one of the major issues hindering accurate measurement of device

17   efficiency, especially for planar heterojunction devices, which often present obvious hysteresis[28].

18   We found that both $PbI_2/PbCl_2$ and PbI_2-based device show a certain degree of hysteresis. The

19   reverse scanning efficiency was higher than the forward scanning efficiency, and the scanning rate

20   impacted hysteresis. Figure S12 shows that the device demonstrates the smallest hysteresis at a

21   scanning rate of 0.1 V/s. Hysteresis was aggravated when the scanning rate was higher or lower

22   than this value. This phenomenon may be related to the device structure and fabrication process[28].

23   Independent of the *PCE* of the device, all of the *J-V* curves presented crosses, which are caused by

24   overestimation of J_{sc} during forward scanning or underestimation of J_{sc} during reverse scanning

25   (Figure S13). This characteristic may be relevant to the grain size of the perovskite according to a

26   previous report[29]. The variation in *PCE* at 0.1 V/s scanning rate was generally within 2%. Thus,

27   this condition was employed in typical characterizations. In order to better evaluate our device

28   performance, we took the steady-state measurements and the results is given in the Figure S14. No

apparent difference PCE acquired from the steady-state measurement and from J-V plot was found. During the steady-state measurement we found the current fast raised when the device was first exposure to the light and declined about 3.2% during the 180s measurement process. The decline of the photocurrent might because of the inferior stability under the ambient measurement condition.

In summary, $PbCl_2$ is an effective additive for organolead trihalide perovskite thin films. $PbCl_2$ inhibited crystallization of PbI_2, resulting in complete conversion of PbI_2 and improvement of the perovskite morphology. Addition of $PbCl_2$ resulted in the formation of $CH_3NH_3PbI_{3-x}Cl_x$ and remarkably prolonged the photoluminescence lifetime, which implies enhancements in transport property. A suitable spin-coating temperature enabled enlargement of the perovskite grain size, thereby enhancing both FF and J_{sc}, which are crucial for high-efficiency devices. Thus, addition of $PbCl_2$ to the PbI_2 DMF precursor solution is a simple and potent method to achieve highly efficient heterojunction perovskite solar cells.

References:

1. H. Kim, C. Lee, J. Im, K. Lee, T. Moehl, A. Marchioro, S. Moon, R. Humphry-Baker, J. Yum, J. E. Moser, M. Grätzel and N. Park, *SCI REP-UK*, 2012, **2**.

2. M. M. Lee, J. Teuscher, T. Miyasaka, T. N. Murakami and H. J. Snaith, *SCIENCE*, 2012, **338**, 643-647.

3. H. Zhou, Q. Chen, G. Li, S. Luo, T. Song, H. Duan, Z. Hong, J. You, Y. Liu and Y. Yang, *SCIENCE*, 2014, **345**, 542-546.

4. L. Etgar, P. Gao, Z. Xue, Q. Peng, A. K. Chandiran, B. Liu, M. K. Nazeeruddin and M. Gra¨tzel, *J AM CHEM SOC*, 2012, **134**, 17396-17399.

5. J. M. Ball, M. M. Lee, A. Hey and H. J. Snaith, *ENERG ENVIRON SCI*, 2013, **6**, 1739.

6. W. A. Laban and L. Etgar, *ENERG ENVIRON SCI*, 2013, **6**, 3249-3253.

7. M. Peng and D. Zou, *J MATER CHEM A*, 2015, **3**, 20435-20458.

8. M. Liu, M. B. Johnston and H. J. Snaith, *NATURE*, 2013, **501**, 395-398.

9. K. Liang, D. B. Mitzi and M. T. Prikas, *CHEM MATER*, 1998, **10**, 403-411.

10. J. Burschka, N. Pellet, S. Moon, R. Humphry-Baker, P. Gao, M. K. Nazeeruddin and M. Grätzel, *NATURE*, 2013, **499**, 316-319.

11.   Z. Xiao, Q. Dong, C. Bi, Y. Shao, Y. Yuan and J. Huang, *ADV MATER*, 2014, **26**, 6503-6509.

12.   Q. Chen, H. Zhou, Z. Hong, S. Luo, H. Duan, H. Wang, Y. Liu, G. Li and Y. Yang, *J AM CHEM SOC*, 2013, **136**, 622-625.

13.   Y. Li, J. K. Cooper, R. Buonsanti, C. Giannini, Y. Liu, F. M. Toma and I. D. Sharp, *The Journal of Physical Chemistry Letters*, 2015, **6**, 493-499.

14.   M. Ibrahim Dar, M. Abdi Jalebi, N. Arora, T. Moehl, M. Grätzel and M. K. Nazeeruddin, *ADV MATER*, 2015, **27**, 7221-7228.

15.   Y. Wu, A. Islam, X. Yang, C. Qin, J. Liu, K. Zhang, W. Peng and L. Han, *ENERG ENVIRON SCI*, 2014, **7**, 2934-2938.

16.   S. D. Stranks, G. E. Eperon, G. Grancini, C. Menelaou, M. J. Alcocer, T. Leijtens, L. M. Herz, A. Petrozza and H. J. Snaith, *SCIENCE*, 2013, **342**, 341-344.

17.   P. Docampo, F. C. Hanusch, S. D. Stranks, M. Döblinger, J. M. Feckl, M. Ehrensperger, N. K. Minar, M. B. Johnston, H. J. Snaith and T. Bein, *ADV ENERGY MATER*, 2014, **4**.

18.   L. H. Brixner, H. Chen and C. M. Foris, *J SOLID STATE CHEM*, 1981, **40**, 336-343.

19.   S. Colella, E. Mosconi, P. Fedeli, A. Listorti, F. Gazza, F. Orlandi, P. Ferro, T. Besagni, A. Rizzo, G. Calestani, G. Gigli, F. De Angelis and R. Mosca, *CHEM MATER*, 2013, **25**, 4613-4618.

20.   H. Yu, F. Wang, F. Xie, W. Li, J. Chen and N. Zhao, *ADV FUNCT MATER*, 2014, **24**, 7102-7108.

21.   M. I. Dar, N. Arora, P. Gao, S. Ahmad, M. Grätzel and M. K. Nazeeruddin, *NANO LETT*, 2014, **14**, 6991-6996.

22.   A. Poglitsch and D. Weber, *The Journal of Chemical Physics*, 1987, **87**, 6373.

23.   W. Nie, H. Tsai, R. Asadpour, J. C. Blancon, A. J. Neukirch, G. Gupta, J. J. Crochet, M. Chhowalla, S. Tretiak, M. A. Alam, H. L. Wang and A. D. Mohite, *SCIENCE*, 2015, **347**, 522-525.

24.   J. Yan and B. R. Saunders, *RSC ADV*, 2014, **4**, 43286-43314.

25.   G. Xing, N. Mathews, S. Sun, S. S. Lim, Y. M. Lam, M. Grätzel, S. Mhaisalkar and T. C. Sum, *SCIENCE*, 2013, **342**, 344-347.

26.   G. E. Eperon, V. M. Burlakov, P. Docampo, A. Goriely and H. J. Snaith, *ADV FUNCT MATER*, 2014, **24**, 151-157.

27.   A. Abrusci, S. D. Stranks, P. Docampo, H. Yip, A. K. Y. Jen and H. J. Snaith, *NANO LETT*, 2013, **13**, 3124-3128.

28.   E. L. Unger, E. T. Hoke, C. D. Bailie, W. H. Nguyen, A. R. Bowring, T. Heumüller, M. G. Christoforo and M. D. McGehee, *Energy Environ. Sci.*, 2014, **7**, 3690-3698.

29.   H. J. Snaith, A. Abate, J. M. Ball, G. E. Eperon, T. Leijtens, N. K. Noel, S. D. Stranks, J. T. Wang, K. Wojciechowski and W. Zhang, *The Journal of Physical Chemistry Letters*, 2014, **5**, 1511-1515.

PbCl$_2$ is used as an additive to assist perovskite film formation in two-step sequential deposition and the device achieved an average efficiency enhancement of approximately 30% compared to the control group.